

## Recycling of Yttria stabilized Zirconia waste powders in glazes suitable for ceramic tiles

Journal:	<i>International Journal of Applied Ceramic Technology</i>
Manuscript ID	ACT-3972.R2
Manuscript Type:	Article
Date Submitted by the Author:	n/a
Complete List of Authors:	Siligardi, Cristina; University of Modena and Reggio Emilia, Department of Engineering of Modena Barbi, Silvia; University of Modena and Reggio Emilia, Department of Engineering of Modena Casini, Roberto; Fritta Italia S.r.l. Tagliaferri, Luca; Turbocoating S.p.A. Remigio, Vito; Ceramica Fondovalle S.p.A.
Keywords:	waste disposal, glazes, zirconia: yttria stabilized

SCHOLARONE™  
Manuscripts

Review

## Recycling of Yttria stabilized Zirconia waste powders in glazes suitable for ceramic tiles

C. Siligardi\*, S. Barbi\*, R. Casini<sup>§</sup>, L. Tagliaferri<sup>°</sup>, V. Remigio<sup>#</sup>

\*Department of Engineering “Enzo ferrari” Via Vivarelli 10/1 41125 Modena, Italy

<sup>§</sup> Fritta Italia SrL, GVia della Stazione 31, Fiorano Modenese (MO), Italy

<sup>°</sup>Turbocoating SpA, Via Mistrali 7, 43040 Rubbiano di Solignano (PR), Italy

<sup>#</sup> Ceramica Fondovalle 12 Via Rio Piodo, 41053 Torre Maina, (MO), Italy

### Abstract

The aim of this work is demonstrate the feasibility of valorizing and recycling Yttria stabilized Zirconia (YSZ) thermal spray waste into high value products for industrial and residential use. Based on the powders chemistry and morphology, this work aims to realize products, like frits suitable for white glazes and ceramic tiles. The focus is on one class of powder: high temperature and abrasion resistant ceramics, like Yttria stabilized zirconia. This study has revealed that the substitution of pure zirconia with waste Yttria stabilized zirconia is possible in high percentages, up to 100% to prepare frits suitable for white glazes.

**Keywords:** waste disposal, glazes, zirconia: yttria stabilized

### 1. Introduction

Nowadays the recycling and reuse of ceramic materials is even more important not only because of the environmental issue but also because of the high cost of mining and transport of pure raw material. In fact this general topic has already been taken into account from a high number of studies [1]. The present study has the aim to develop in detail the recycling of Yttria stabilized Zirconia (YSZ) waste powders from thermal barrier coating application to traditional ceramic

1  
2  
3 tiles.

4  
5 In particular, considering the commercial frits, suitable for single-fast firing of ceramic tile, those  
6  
7 containing zircon ( $ZrSiO_4$ ) and zirconia ( $ZrO_2$ ) are of great interest, and are commonly named as  
8  
9 “white of zirconium” [2]. Generally the composition of this category of frits is characterized by  
10  
11 50-60 wt% of  $SiO_2$ , 8-14wt% of  $ZrO_2$ , 20-25wt% of fluxing elements such as  $Na_2O$ ,  $K_2O$ , and  
12  
13  $B_2O_3$  and 7-9wt% of stabilizing elements such as  $ZnO$ ,  $Al_2O_3$ ,  $CaO$ ,  $BaO$ ,  $MgO$  as minor  
14  
15 components [2].  $ZrSiO_4$  was proved to promote opacity, as whitening agent, in presence of  $ZnO$   
16  
17 and providing that the  $SiO_2/Al_2O_3$  molar ratio is equal to 10 [3-6]. The mechanism behind the  
18  
19 peculiar optical properties of  $ZrSiO_4$  is due to the particle size of zircon crystals that approaches  
20  
21 the wavelength of incoming light enhancing light scattering and, thus, opacification [7].  $ZrSiO_4$   
22  
23 can be included as  $ZrO_2$  in the frit where the combination with excess silica led to the formation  
24  
25 of zircon crystals, that promotes opacification regardless the zirconium compound employed in  
26  
27 the glaze formulation [7-8]. The glazes developed from that frits category may have different  
28  
29 surface appearance, according with other frits or raw material inside the glazes formulation, such  
30  
31 as glossy or opaque. More details about the chemical properties and microstructure of zirconium  
32  
33 glazes can be found in previous works [7,9-10]. Moreover, Zircon is generally imported in  
34  
35 Europe from Australia or South Africa [11], increasing the cost of this material and contributing  
36  
37 to market speculation with an high cost fluctuation [6,11]  
38  
39  
40  
41  
42  
43  
44

45 Zirconia is a very important industrial ceramic material for structural applications due to its high  
46  
47 toughness at high temperature. Zirconia has found use mainly in oxygen pumps and sensors, fuel  
48  
49 cells and thermal barrier coatings. However, most engineering applications make use of the  
50  
51 tetragonal and cubic phases obtained through the stabilization or partial stabilization of the  
52  
53 tetragonal forms, through the introduction of dopants such as  $Y_2O_3$  oxide [12]. Yttria Stabilized  
54  
55 Zirconia (YSZ) is one of the most widely used ceramic materials for TBC applications because of  
56  
57  
58  
59  
60

1  
2  
3 its low thermal conductivity, high-temperature stability in oxidizing and reducing environments,  
4  
5 coefficient of thermal expansion similar to Ni/Co based super-alloys, high toughness, and cost-  
6  
7 efficiency, by which it can be applied onto metal surfaces. Yttria Stabilized Zirconia (YSZ) can  
8  
9 be found in combustor liners, transition sections, nozzle guide vanes, and rotor blades for gas  
10  
11 turbine applications [12]. Yttria stabilized zirconia has been established as standard material for  
12  
13 the top coat in thermal barrier coating in the last years through thermal spray technology [13-15].  
14  
15 In general the processes consists of injecting a feedstock material (in powder form, seldom as  
16  
17 wire) into a hot gas stream generated by a thermal spray torch. The stream heats the powder  
18  
19 particles (or melts the wire tip, removing liquid droplets) and drags them towards a target  
20  
21 substrate, where they impinge at high temperature and velocity. The coating is therefore built up  
22  
23 by the superposition of various layers of flattened particles (often called “lamellae” or “splats”)  
24  
25 as the torch, usually controlled by an industrial robot, traverses repeatedly in front of the  
26  
27 substrate. [16]

28  
29 Specifically, the TURBOCOATING SpA (Rubbiano di Solignano, Italy) company involved in  
30  
31 this research focuses on aeronautics (gas turbine aircraft engines) and energy production  
32  
33 (industrial gas turbines) coating applications. Turbocoating applies ceramic coatings, in particular  
34  
35 Yttria Stabilized Zirconia (YSZ) for thermal insulation and erosion protection, by atmospheric  
36  
37 plasma spraying. In the same spray booths used for ceramic coating also low pressure plasma  
38  
39 spraying and high velocity oxygen-fuel spraying are employed to produce Ni- and Co- based  
40  
41 alloy coatings (NiCoCrAlY alloys) for oxidation and hot corrosion protection.  
42  
43  
44  
45  
46  
47  
48  
49

50  
51 In all cases, thermal spray processes run in enclosed environments (spray booths) attached to  
52  
53 exhaust systems equipped with dust separation filters. From the environmental point of view, one  
54  
55 of the main problems of this technology is that during the spraying process, a significant fraction  
56  
57 of the powders is indeed not deposited onto the substrate. Due to the stochastic nature of the  
58  
59  
60

1  
2  
3 particle injection and treatment inside gas flows, some particles may reach the substrate with  
4 inadequate velocity and/or temperature, which results in their rebounding off the target upon  
5 impact, without deposition. As a result, a fraction of the feedstock powder usually ranging from  
6 50% up to 80% is not deposited onto the substrate, and it is either collected at the booth floor or  
7 inside the dust filters. These spent powders are not re-usable in the thermal spray process itself,  
8 because of various reasons. In particular because these spent powders may have been deformed  
9 and/or fragmented, so that the shape and size distribution of the spent powder particles is usually  
10 altered compared to the original ones, which is unacceptable for a thermal spray process, where a  
11 very precisely controlled particle size distribution is needed to maintain the desired coating  
12 quality and reproducibility. Moreover, powder contamination may arise from a variety of sources,  
13 including wear of the powder feeding and spraying equipment, wear of the exhaust and dust  
14 collection system, detachment of debris or fragments from the substrate, etc. The powders that  
15 have fallen down in the spraying booth after spraying is collected from the ground or from the air  
16 filters and must be treated as waste. Presently, the powders collected in the booth and/or in the  
17 dust collection system are treated as “special waste” and, due to the presence of elements such as  
18 Ni, Co or other heavy metals (contributed by the powder itself and/or by contaminations), they  
19 are labeled as hazardous, which increases the complexity and costs of their disposal and eventual  
20 dumping [17].  
21  
22  
23  
24  
25  
26  
27  
28  
29  
30  
31  
32  
33  
34  
35  
36  
37  
38  
39  
40  
41  
42  
43  
44

45 The aim of this work is to characterize and reuse spent feedstock YSZ powders recovered at the  
46 end of various thermal spray processes by TURBOCOATING SpA. In the first part of this study  
47 two overspray zirconia powders, coming from two different spray boots, has been characterized  
48 in order to analyze particle morphology, size distribution, color, chemical and phase composition.  
49 Through these results, the contaminations level introduced by the thermal spray processing has  
50 been identified and suitable classification and purification methods have been studied. Different  
51  
52  
53  
54  
55  
56  
57  
58  
59  
60

1  
2  
3 fraction of the purified powder has been characterized subsequently in order to verify the  
4  
5 contamination level obtained after the cleaning process. The best fractions, in terms of chemical  
6  
7 purity and homogenous particle morphology and distribution, have been employed to formulate  
8  
9 industrial frits suitable for white glazes with a substitution up to 100% of pure zirconia with  
10  
11 purified overspray zirconia. These new frits have been compared with an industrial standard frit  
12  
13 suitable for white glazes. Subsequently three different glazes has been prepared using the new  
14  
15 frits and compared with industrial standard white glaze.  
16  
17

18  
19  
20 This paper regards the continuous of the study published in 2014 by Siligardi et al. [18] where the  
21  
22 substitution of pure zirconia with waste zirconia in a ceramic glaze, was possible only in small  
23  
24 percentages due to the presence of chromophore ions into waste zirconia, which tend to color the  
25  
26 glaze.  
27  
28

## 29 30 31 32 2. Materials and Methods

33  
34 Two different YSZ overspray waste powders were delivered from Turbocoating SpA. Samples,  
35  
36 labeled as Z1AR (Zirconia 1 as received) and Z2AR (Zirconia 2 as received), came from two  
37  
38 different spraying booths. Z1AR comes from a spray booth where 5% of the working time is  
39  
40 employed for the spraying of the metallic bond coat, whereas the rest of the working time of the  
41  
42 plant is dedicated to the spraying of the ceramic top coat. On the contrary, Z2AR comes from a  
43  
44 spray booth where 20% of the working time is employed for the spraying of the metallic bond  
45  
46 coat, and the rest of the time is employed for the ceramic top coat. These two booths have their  
47  
48 own downstream filtering system that collects all the oversprayed powder generated during the  
49  
50 deposition process. The powders Z1AR and Z2AR are thus collected from these filtering  
51  
52 systems.  
53  
54  
55  
56  
57  
58  
59  
60

1  
2  
3 In the first part of the work, Z1AR and Z2AR were investigated by using X-Ray Fluorescence  
4 (XRF, ADVANT'XP+, Thermo ARL), X-ray diffraction (XRD, PW3710, Philips), scanning  
5  
6 electron microscopy (SEM, FEI XL-30). The analysis of the particle size distribution of the as  
7  
8 received powders was performed by using the laser diffraction method (Mastersizer 2000 particle  
9  
10 size analyzer with Hydro-S wet dispersion unit, Malvern Instrument Ltd., Malvern UK). The  
11  
12 analysis of the color of the powders was performed by measuring the colorimetric CIEL\*a\*b\*  
13  
14 parameters (XP62, X-Rite), using D65 illuminant and CIE 1931 2° observer, following the CIE  
15  
16 recommendations and the ASTM E308-85 [19,20]. L\* describes the brightness of the color (L\*  
17  
18 = 0 for black; L\* = 100 for white), a\* describes the red (a\* = 120) - green (a\* = -120) component  
19  
20 and b\* describes the yellow (b\* = 120) -blue (b\* = -120) component of the color. The colors have  
21  
22 been compared through the calculation of  $\Delta E$  parameter [19].  
23  
24  
25  
26  
27  
28

29 Subsequently, physical treatments of sieving were performed in order to separate pure zirconia  
30  
31 from pollutant particles. The sieving was performed through a set of vibrational laboratory  
32  
33 machine (Retsch, AS200), using three different sieves in column (38, 45 and 75  $\mu\text{m}$ ), for a  
34  
35 vibration time of 8 hours.  
36  
37

38 After the sieving, all the fraction of both the as received powders has been characterized  
39  
40 following the same procedure done for the as received powders.  
41  
42

43 After characterization of all the fractions, the purest powders have been collected by FRITTA  
44  
45 ITALIA S.r.l (Fiorano Modenese, Italy) in order to prepare frits and glazes, starting from a  
46  
47 standard formulation for white frits and glazes. Table 1 shows the standard frit chemical  
48  
49 compositions taken in account in this work.  
50  
51

52 Replacements of 100% of the pure zircon were performed in the white frit employing the purest  
53  
54 recycled powders fraction and industrial quartz as source of  $\text{SiO}_2$ . The frits obtained were named  
55  
56  
57  
58  
59  
60

1  
2  
3 Z1-F and Z2-F respectively coming from the purest fractions of Z1AR and Z2AR. The frits  
4  
5 preparation was performed mixing the raw material reported in the table 1 and melting the batch  
6  
7 at 1500°C in an industrial kiln. The liquid melts were quenched in water to obtain frits. In order  
8  
9 to identify the characteristic points of sintering, softening, sphere, half-sphere and melting, a hot-  
10  
11 stage microscopy analysis was performed on the frits (Expert System Solutions, Misura HSM) at  
12  
13 the heating rate of 10°C/min until 1200°C [21]. In order to verify the color of the frits they were  
14  
15 applied onto a green porcelainized stoneware body through an airbrush following the procedure  
16  
17 already reported in the previous study [18]. The color of the frits, after application on the ceramic  
18  
19 substrate was measured with the same method used for the powders.  
20  
21  
22  
23

24  
25 The frits were mixed with others industrial raw material as shown in Table 2, and water in an  
26  
27 industrial mill, in order to obtain the glazes: STD-GG indicate the standard glossy glaze, whereas  
28  
29 STD-OG indicate the standard opaque glaze. Considering the formulations as shown in Table 2  
30  
31 the frit taken in account for the **substitution** of the raw material with the waste powders is named  
32  
33 as “Frit”, and also the zircon as raw material has been substituted with a **stoichiometric**  
34  
35 combination of silica and waste zirconia.  
36  
37

38  
39 The slurries were deposited on a dry green ceramic support by airless method by Ceramica  
40  
41 Fondovalle (Torre Maina, Italy). The ceramic tiles were fired in an industrial kiln for 54 minutes,  
42  
43 reaching the maximum temperature of 1215°C. The characterization of the glazes was performed  
44  
45 using a multiple techniques approach. The crystalline phases formed in the samples were  
46  
47 identified by X-ray diffraction (XRD, PW3710, Philips) and scanning electron microscope (SEM,  
48  
49 FEI XL-30). The analysis of the color of the glazes was performed by measuring the colorimetric  
50  
51 CIEL\*a\*b\* parameters (XP62, X-Rite), using D65 illuminant and CIE 1931 2° observer,  
52  
53 following the ASTM E 308-85 [19,20]. Spectral reflectance of each sample was measured using a  
54  
55 UV-Vis-NIR spectrophotometer (Jasco V 670) with a 150 mm integrating sphere, in  
56  
57  
58  
59  
60

1  
2  
3 accomplishment to ASTM E903 (ASTM International PA, 2004). The solar reflectance value  $\rho_{\text{sol}}$   
4  
5 of every surface was calculated by integrating over the range from 300 to 2500 nm the measured  
6  
7 spectral reflectivity  $\rho_{\lambda}$  (defined as the ratio of reflected part and total amount of incident radiation  
8  
9 at the considered wavelength  $\lambda$ ), weighted by the standard spectral irradiance of the sun at the  
10  
11 earth surface,  $I_{\text{sol},\lambda}$  [ $\text{Wm}^{-2} \text{nm}^{-1}$ ] described by the AM1GH irradiance spectrum [22].  
12  
13  
14  
15  
16

### 17 3.Results and discussion

#### 20 3.1 As received zirconia powders characterization

21  
22 The particle size analysis of the as-received overspray zirconia revealed a monomodal grain size  
23  
24 distribution as shown in Figure 1 and Figure 2 for Z1AR and Z2AR respectively. The grain size  
25  
26 parameters D10, D50 and D90 are shown in Table 3 for both the samples. Considering the results  
27  
28 as presented in Table 3 and Figure 1 and Figure 2 , the particle size distribution of zirconia waste  
29  
30 powders are coarser than pure zirconium silicate used in the ceramics industry, which usually  
31  
32 presents a D50 value of around 10 microns. Moreover the sample Z2AR show a widespread grain  
33  
34 size distribution, in respect of Z1AR.  
35  
36  
37  
38  
39

40 The chemical analyses of the samples are shown in Table 3. Powder Z2AR contains higher  
41  
42 amount of chromophore oxides than Z1AR, since it shows Ni, Co and Cr oxides. The presence of  
43  
44 these oxides in Z2AR is probably due to the fact that from that spray booth a more polluted  
45  
46 powder is collected, since more working time is dedicated to the spraying of the metallic bond  
47  
48 coat. In Table 3 also the colorimetric parameters are shown. These parameters confirms in part  
49  
50 the results of the chemical analysis, because Z2AR that is the sample with the highest amount of  
51  
52 chromophore ions it is also the darker one, because the  $L^*$  value is lower that the  $L^*$  value of  
53  
54 Z1AR sample. The XRD patterns of both the samples are the same, as can be seen in Figure 3  
55  
56  
57  
58  
59  
60

1  
2  
3 and Figure 4 respectively, so no difference in the level of pollutant can be detected with X-Ray  
4  
5 diffraction. The general results for both the samples are that the powders are composed mainly by  
6  
7 tetragonal Zirconia. This crystalline phase shows also two double peaks, as highlighted in the  
8  
9 circles in Figure 3 and Figure 4, that are associated with crystalline phases that underwent to a  
10  
11 thermal spray process, as previously reported [18].  
12  
13

14  
15 Figure 5 and Figure 6 show the SEM images of Z1AR and Z2AR respectively at two different  
16  
17 magnification 800X and 2000X. The SEM observation of as received zirconia reveals the  
18  
19 presence of spherical, agglomerated and irregular shaped grains; moreover broken grains and  
20  
21 pieces of sintered powders are present as well. From the characterization collected at this point  
22  
23 Z2AR sample shows a higher presence of some contamination particles, due to the different  
24  
25 coloration and morphology, with respect of pure zirconia powders.  
26  
27  
28  
29  
30  
31  
32  
33  
34  
35

### 36 3.2 Sieved zirconia powders characterization

37  
38  
39 Table 4 shows the parameters analyzed for the sieved fraction of Z1AR. For first the grain size  
40  
41 parameters of all the sieved fraction confirms the effectiveness of the sieving, because, for each  
42  
43 fraction of powder, D90 is more or less equal to the dimension of the following sieve. Moreover  
44  
45 is important to underline that the fraction with the higher amount of sieved powder is the one <38  
46  
47  $\mu\text{m}$ . This fraction is also the less polluted from metallic oxides, considering the higher amount of  
48  
49  $\text{ZrO}_2$  in the XRF results, and the brighter one in color, considering its highest value of  $L^*$ . The  
50  
51 powders <38  $\mu\text{m}$  and >38  $\mu\text{m}$  show similar data, in this case the sieving process does not strongly  
52  
53 increase the purity of the powders, in fact we have to consider the instrumental error of the XRF  
54  
55  
56  
57  
58  
59  
60

1  
2  
3 technique that is 0.3 wt%. In particular observing the optical microscopy images, the amount of  
4  
5 contamination particle decrease in the powder sieved through 45 $\mu$ m sieve. This means that the  
6  
7 black particles have more or less dimension higher than 45  $\mu$ m, so it is possible to “clean” the as-  
8  
9 receive powders. This result is also confirmed by the chemical analysis of the sieved powders. In  
10  
11 fact it is possible to observe that lower is the particle size, higher is the purity of the waste  
12  
13 zirconia. decreasing the particle size distribution the purity of the waste zirconia increase.  
14  
15  
16 Moreover the color is depending on the grain size distribution, also visible in the optical image,  
17  
18 and confirmed by CIELab parameters. Considering all this results, for Z1AR we can assess that  
19  
20 the fractions < 38  $\mu$ m and >38  $\mu$ m are the cleanest and can be used to formulate frits suitable for  
21  
22 white glaze. These fractions together collect the 69.16% of Z1AR as shown in Table 4.  
23  
24  
25

26  
27 Table 5 shows the parameters analyzed for the sieved fraction of Z2AR. Also in this case the  
28  
29 grain size parameters of all the sieved fraction confirms the effectiveness of the sieving, because,  
30  
31 for each fraction of powder, D90 is more or less equal to the dimension of the following sieve. In  
32  
33 spite of Z1AR, the fractions of Z2AR with the higher amount of sieved powder are >38  $\mu$ m and  
34  
35 >45 $\mu$ m. Also in this case the sieved fraction < 38 $\mu$ m is the less polluted from metallic oxides,  
36  
37 considering the higher amount of ZrO<sub>2</sub> but also the lower content of the chromophore cobalt  
38  
39 oxide in the XRF results. Also for Z2AR sieved fraction it is possible to observe that decreasing  
40  
41 the particle size distribution the purity of the waste zirconia increases. Moreover, also the colour  
42  
43 is depending on the grain size distribution, as well visible in the optical image, and confirmed by  
44  
45 CIELab parameters. As for Z1AR powder the amount of contamination particle decrease in the  
46  
47 powder sieved through 45 $\mu$ m, for Z2AR the amount of pollutant decrease significantly in the  
48  
49 powder sieved <38  $\mu$ m. Considering all this results, for Z2AR we can assess that the fraction <  
50  
51 38  $\mu$ m is the cleanest and can be employed to formulate frits suitable for white glaze. This  
52  
53  
54  
55  
56  
57  
58  
59  
60

1  
2  
3 fraction collects the 13.21% of Z2AR as shown in Table 5. As a result, considering the amount of  
4  
5 the cleanest powder sieved for Z1AR and for Z2AR we expect to recover less clean powder from  
6  
7 Z2AR than Z1AR.  
8  
9

### 10 11 12 3.3 Frits and glazed tiles characterization

13  
14  
15 In Table 6 the hot stage microscope characterization of the two studied frits has been shown, in  
16  
17 comparison with the data of the standard frits. It can be observed that the thermal behavior (see  
18  
19 characteristic temperatures) of the new frits containing the purest fraction of waste zirconia  
20  
21 instead of pure raw material is quite similar to the behavior shown by the standard industrial frits,  
22  
23 independently from the type of waste zirconia employed (Z1-F or Z2-F). For this reason we can  
24  
25 assume that the thermal behavior of the glazes during firing will be similar and no further  
26  
27 changes will be necessary to employ these frits in industrial application. The reasons for this  
28  
29 claim are principally two: the first reason is that we must consider that the materials taken in  
30  
31 consideration in this study are industrial materials, that work at quite high temperature in  
32  
33 industrial kiln, where a variation range of  $\pm 50^{\circ}\text{C}$  must be considered as acceptable. The second  
34  
35 reason is that when glazes for ceramic tile are studied generally sphere, half-sphere and melting  
36  
37 are the most important temperature to be evaluated and compared. For this reason, higher  
38  
39 discrepancy for sintering and softening can be evaluated as secondary.  
40  
41  
42  
43  
44

45  
46 In table 7 the results obtained through the color measurement of the frits have been shown after  
47  
48 the application on ceramic support. From this results we can observe that a relevant decrease can  
49  
50 be seen for  $L^*$  coordinate and a significantly increase can be estimated for  $b^*$  coordinate. A  
51  
52 strong difference in terms of color can be observed when Z2-F is compared with the white  
53  
54 standard frit.  
55

56  
57 In Figure 7 a comparison of the glossy glazes obtained with STD-F, Z1-F and Z2-F respectively,  
58  
59  
60

1  
2  
3 following the composition shown in Table 2, is shown. From Figure 7 it is possible to see that  
4  
5 Z1-GG is white and no coloration is shown if compared with the standard white glaze. On the  
6  
7  
8 contrary Z2-GG has shown a strong greenish coloration. Similar results can be achieved using the  
9  
10 same frits to produce opaque glazes as shown in Figure 8. The change in coloration can be  
11  
12 measured and is confirmed through the color parameters as shown in Table 8.

13  
14 Considering Table 8 and the values obtained from Z2-GG and Z2-OG a strong decrease can be  
15  
16 seen for L\* coordinate and a relevant increase can be estimated for b\* coordinate, both for glossy  
17  
18 and opaque glaze. These differences indicate respectively a decrease in brightness and an  
19  
20 increase in the greenish tone. ~~About color~~ Also the  $\Delta E$  value can be observed, in order to  
21  
22 consider an objective measurement of the difference in color **between a glaze and its reference.**

23  
24  
25  
26  
27 -Higher is the  $\Delta E$  value and higher is the difference between the two colors compared.  $\Delta E$  value  
28  
29 in the case of Z1-GG is 1.54 that is below the limit of acceptance for the human eye ( $\Delta E = 3$ )  
30  
31 [23], for this reason the two colors can be estimated as the same. On the contrary the  $\Delta E$  value  
32  
33 associated with Z2-GG is 18.11, so strongly over the limit of acceptance for the human eye. The  
34  
35 same evaluations can be done for Z1-OG and Z2-OG respectively. The change in coloration can  
36  
37 be explained considering the presence of chromophore elements in the sieved powders employed  
38  
39 in Z2-F frit, as cobalt and chromium in particular, even if present in low amount as shown in  
40  
41 Table 5 [24-25]. Taking in account the light greenish coloration achieved we can assume also that  
42  
43 in this case cobalt ion is 4-fold coordinated [26]. Considering this result, the frit formulated with  
44  
45 the sieved fraction of Z2AR powder must be discarded because, even if low, the amount of  
46  
47 metallic pollutant prevents the achievement of a white glaze. Because of this result the further  
48  
49 characterizations have been done only on the white glazes obtained Z1-GG and Z1-OG. The  
50  
51 reflectance spectra of the white glazes obtained are shown in Figure 9 and Figure 10 considering  
52  
53 respectively glossy and opaque glaze.  
54  
55  
56  
57  
58  
59  
60

1  
2  
3 From Figure 9 and Figure 10 it is possible to see that the reflectance spectra of the glazes are  
4 overlapped in both cases in the visible region (400-700nm), no relevant changes can be seen for  
5  
6 this property when pure zircon is substitute with the sieved fraction of Z1AR and quartz.  
7  
8

9  
10 In order to evaluate any change in microstructure XRD and SEM measurement has been  
11 performed on all the white glaze samples obtained. In Figure 11 the XRD pattern of the samples  
12  
13 STD-GG and Z1-GG have been shown.  
14  
15

16  
17 About the glossy samples shown in Figure 11 it is possible to see that both the pattern are  
18 characterized by a strong glassy band and the only one mineralogical phase identified is Zircon  
19 (ICDD: 01-083-1374), in fact all the peaks present in the patterns shown in Figure 11 can be  
20 associated with that mineralogical phase. In Figure 12 the XRD pattern of the samples STD-OG  
21 and Z1-OG have been shown.  
22  
23  
24  
25  
26  
27  
28  
29  
30

31 About the opaque samples, as shown in Figure 12 it is possible to achieve that the mineralogical  
32 phases are two: Zircon (ICDD: 01-083-1374) and Anorthite (ICDD:00-018-1202). The difference  
33 in terms of mineralogical phases between glossy and opaque glaze is due to different raw material  
34 inside the glaze employed to obtain the desired surface appearance. Also an important difference  
35 in terms of glassy phases is present, in fact as expected the glassy phases in higher for the glossy  
36 glazes in respect of the opaque ones. This result can be evaluated observing the band around 25-  
37 27 °2θ, that is typically associated with the presence of silicate glassy phase. As expected from  
38 other studies [27] X-ray diffraction studies that have examined glazes containing both zircon and  
39 zirconia have demonstrated that zircon is the final opacifier crystal, regardless of which  
40 zirconium species is present in the glaze formulation. Other researches have shown that the  
41 amount of zircon or zirconium oxide that forms initially is dependent on the SiO<sub>2</sub>:ZrO<sub>2</sub> ratio in  
42  
43  
44  
45  
46  
47  
48  
49  
50  
51  
52  
53  
54  
55  
56  
57  
58  
59  
60

1  
2  
3 the frit. Glazes with lower silica contents have a tendency, initially, to produce zirconium oxide  
4  
5 phases, whereas higher silica glazes initially produce zircon crystals during heating. In both  
6  
7 cases, however, zircon was, again, the major opacifier phase in the final glaze. In Figure 13 and  
8  
9 Figure 14 respectively the SEM images of the glossy and opaque glazes respectively has been  
10  
11 shown.  
12  
13

14  
15 The SEM images considered are in backscattered electron in order to identify the presence of  
16  
17 crystals inside the microstructure of the glazes. The SEM images obtained from the samples Z1-  
18  
19 GG and Z1-OG are completely similar to respectively STD-GG and STD-OG. This result  
20  
21 demonstrates that the substitution of pure zirconium silicate with a sieved fraction of YSZ and  
22  
23 quartz does not change the glaze microstructure. As expected, important difference can be  
24  
25 considered if we compare the microstructure of the glossy glaze with the microstructure of the  
26  
27 opaque glaze. As previously seen in the XRD analysis the opaque glaze is characterized by a  
28  
29 strong presence of crystals than the glossy glaze. In particular in Figure 14 that refers to the  
30  
31 opaque glazes analyzed needle-shape crystals and rod-shape crystal can be clearly seen in both  
32  
33 the samples. For similar system, in literature the needle-shape crystals are associated with the  
34  
35 presence of zircon crystals [28-30], whereas the rod-shape crystals can be associated with  
36  
37 Anorthite [6]. On the contrary, in the glossy glazes only zircon crystals can be seen on the  
38  
39 surface, as shown in Figure 13. In fact as shown from the EDS analysis in Figure 15, the crystals  
40  
41 show the chemical composition of zircon, whereas the glassy phase shows the chemical  
42  
43 composition of the glaze. The larger zircon crystal present in the glossy glazes can derive from an  
44  
45 aggregation of zircon that is added in the glaze formulation as raw material as shown in Table 2.  
46  
47  
48  
49  
50  
51  
52  
53 In fact the typical grain size of this industrial powder is about 1,25  $\mu\text{m}$  (D50).  
54  
55  
56  
57  
58  
59  
60

## Conclusion

In this study the feasibility of valorizing and recycling YSZ thermal spray waste, in relevant amount, to high value products as white glazes for ceramic tile has been demonstrated. As shown in previously studies [18] YSZ thermal spray waste cannot be employed in a 100% substitution in frits or glaze for white glaze formulation due to the high amount of metallic pollutant. In this study we have demonstrated that the mechanical action of sieving is effective in order to remove the metallic pollutant from at least 59.16% of the Z1AR thermal spray waste. The purified powder can be employed in a 100% substitution of zirconia, in combination with quartz. In fact, colour measurement, SEM and XRD analysis in particular have shown that the parameters are in the same range of the standard industrial white glazes, both for glossy and opaque types. As confirmed by previous study [26] zircon is the main crystalline phase inside the glaze microstructure, regardless of which zirconium species is present in the glaze formulation.

The analysis of Z2AR, demonstrate that if the pollutant is in too high amount the powder cannot be recycled for white frits and glazes, so other studies will be necessary to find other field of application for this waste powder.

Taking in account only the waste powder from Turbocoating, about 480 Kg is the amount of waste powder that can be recycled for white frits in a month through mechanical sieving. Following the formulations employed in this study this means that the waste powders recycled in one month can cover the production of approximately 480.000 mq of ceramic tiles. As only the Italian production of ceramic tile during 2015 reached 397 millions/mq [31], the recycled powder can cover approximately the 1,33% of only the Italian production of ceramic tile.

As future prospective technological characterizations of the glazes will be done in order to complete the comparison between standard product and product obtained with waste powders.

## Acknowledgments

This study was supported by the European Union through the project LIFE12 ENV/IT/00678, ReTSW-SINT – recycling of thermal spray waste in sintered products.

For Peer Review

## References

1. Rawlings RD, Wu JP, Boccaccini AR. Glass-ceramics: Their production from wastes—A Review. *J. Mater. Sci.* 2006;41:733–761.
2. Romero M, Rincon JM, Acosta A. Crystallization of a zirconium based glaze for ceramic tile coating. *J. Eur. Ceram. Soc.* 2003;23:1629–1635.
3. Parmalee CW. Ceramic Glazes. 3thed. Boston, NY: Cahnners Books; 1973.
4. Shaw K. Ceramic Glazes. Amsterdam, NL: Elsevier Science; 1971.
5. Garcia Sainz J. Physical-chemical characteristics of ceramic glazes and their influence on quality of floor and wall tiles. *Tile Brick Int.* 1990; 6:21-22.
6. Selli NT. Development of anorthite based white porcelain stoneware tile compositions. *Ceram. Int.* 2015;41:7790–7795.
7. Castilone RJ, Sriram D, Carty WM, Snyder RL. Crystallization of zircon in stoneware. *J. Am. Ceram. Soc.* 1999;82:2819–2824.
8. Jacobs CW. Opacifying Crystalline Phases Present in Zirconium-Type Glazes. *J. Am. Ceram. Soc.* 1954;37:216–220.

- 1  
2  
3 9. El-Defrawi SA, Abd El-Fattah WI. Pinholes and introduction of albite in double firing zircon-  
4 glazed tiles. *Silicates Industriels*. 1993;58:31-36.  
5  
6  
7  
8  
9  
10 10. El-Defrawi SA, Serry MA, Abd El-Fattah WI, Weisweiler W. Microchemistry and  
11 microstructure of some opaque glaze/tile interfaces in relation to their physical properties.  
12 *Ceram. Int*. 1995;21:69–75.  
13  
14  
15  
16  
17  
18  
19 11. T.Z. Minerals International Pty Ltd, Zircon supply/demand report. 2016.  
20  
21  
22  
23  
24 12. Shackelford JF, Doremus RH. Ceramic Glass Materials. New York, NY: Springer; 2008.  
25  
26  
27  
28 13. Padture NP, Gell M, Jordan EH. Thermal Barrier Coatings for Gas-Turbine Engine  
29 Applications. *Science*. 2002;296:280–284.  
30  
31  
32  
33  
34  
35 14. Clarke DR, Levi GG. Materials Design for the Next Generation Thermal Barrier Coatings.  
36 *Annu. Rev. Mater. Res*. 2013;33:383–417.  
37  
38  
39  
40  
41  
42 15. Vassen R, Jarligo MO, Steinke T, Mack DM, Stoeber D. Overview on advanced thermal  
43 barriercoatings. *Surf. Coat. Technol*. 2010;205:938–942.  
44  
45  
46  
47  
48 16. Kumar V, Kandasubramanian B. Processing and design methodologies for advanced and  
49 novel thermal barrier coatings for engineering applications. *Particuology*. 2016;27:1–28.  
50  
51  
52  
53  
54 17. Dawson T. A clean spray. *Industrial Paint & Powder*. 2006;6:10-14.  
55  
56  
57  
58  
59  
60

- 1  
2  
3 18. Siligardi C, Lusvarghi L, Giolli C, Scrivani A, Venturelli D. Recycling in ceramic glazes of  
4 zirconia overspray from thermal barrier coatings manufacturing. *J. Eur. Ceram. Soc.* 2014;34:  
5 147–154.  
6  
7  
8  
9  
10  
11 19. Hunt RWG, Pointer MR. *Measuring Colour*. Oxford, UK: John Wiley and Sons; 2011.  
12  
13  
14  
15  
16 20. ASTM E308-85. Standard Practice for Computing the Colors of Objects by Using the CIE  
17 System. West Conshohocken, PA: ASTM International; 1987.  
18  
19  
20  
21 21. Paganelli M. Understanding the behavior of glazes: new test possibilities using the automatic  
22 hot stage microscope MISURA. *Ind. Ceram.* 1997;17:69-73.  
23  
24  
25  
26  
27  
28 22. Levinson R, Akbari H, Berdahl P, Measuring solar reflectance Part I: defining a metric that  
29 accurately predicts solar heat gain, *Solar Energy*, 2010;84:1717-1744.  
30  
31  
32  
33  
34 23. ACIMAC. *Colour, pigments and colouring in ceramics*. Modena, IT: SALA; 2003.  
35  
36  
37  
38 24. Huang M, Wang Z, Liu S. Reutilization of the Cr ions adsorbed on activated carbon as  
39 colorants in glass preparation. *J. Environ. Chem. Eng.* 2016;4:1555-1560.  
40  
41  
42  
43  
44 25. Hunault M, Bauchau F, Loisel C, Herold M, Galois L, Newville M, Calas G. Spectroscopic  
45 Investigation of the Coloration and Fabrication Conditions of Medieval Blue Glasses. *J. Am.*  
46  
47  
48  
49  
50  
51  
52  
53  
54  
55  
56  
57  
58  
59  
60

- 1  
2  
3 26. Paul A, Douglas RW. Optical absorption of divalent cobalt in binary alkali borate  
4 glasses and its relation to basicity of glass. *Phys. Chem. Glasses-Eur. J. Glass Sci.*  
5  
6  
7  
8 *Technol. Part B.* 1968;9:21–26.  
9  
10  
11  
12 27. Sehlke KH, Tauber A.A High-Temperature X-ray Diffraction Study of Zircon-Containing  
13 Glaze Frits. *Trans. Br. Ceram. Soc.* 1969;68:53–56.  
14  
15  
16  
17  
18  
19 28. Sheikhattar M, Attar H, Sharafi S, Carty WM. Influence of surface crystallinity on the surface  
20 roughness of different ceramic glazes. *Mater. Charact.* 2016;118:570–574.  
21  
22  
23  
24  
25  
26  
27 29. Wang S, Peng C, Xiao H, Wu J. Microstructural evolution and crystallization mechanism of  
28 zircon from frit glaze. *J. Eur. Ceram. Soc.* 2015;35:2671–2678.  
29  
30  
31  
32  
33  
34 30. Wang X, Chen M, Zhu S, Wang F. Phase evolution of  $\text{SiO}_2\text{-Al}_2\text{O}_3\text{-ZnO-CaO-ZrO}_2\text{-TiO}_2\text{-}$   
35 based glass with added Y-PSZ particles. *J. Am. Ceram. Soc.* 2013;96:1456–1463.  
36  
37  
38  
39  
40  
41 31. ACIMAC. World production and consumption of ceramic tile. Modena, IT: SALA;2016.  
42  
43  
44  
45  
46  
47  
48  
49  
50  
51  
52  
53  
54  
55  
56  
57  
58  
59  
60

## LIST OF FIGURE CAPTIONS

Figure 1. Grain size distribution of sample Z1AR

Figure 2. Grain size distribution of sample Z2AR

Figure 3. XRD Pattern of sample Z1AR: t-Zr, tetragonal zirconia

Figure 4. XRD Pattern of sample Z2AR: t-Zr, tetragonal zirconia

Figure 5. SEM Images at different magnitude of sample Z1AR

Figure 6. SEM Images at different magnitude of sample Z2AR

Figure 7. Comparison of the glossy glazes obtained a) STD-GG b) Z1-GG c) Z2-GG

Figure 8. Comparison of the opaque glazes obtained a) STD-OG b) Z1-OG c) Z2-OG

Figure 9. Reflectance spectra of the white glossy glazes

Figure 10. Reflectance spectra of the white opaque glazes

Figure 11. XRD Pattern of the white glossy glazes: Zr-Si, Zirconium Silicate

Figure 12. XRD Pattern of the white opaque glazes: Zr-Si, Zirconium Silicate; A, Anorthite

Figure 13. SEM Images of sample a) STD-GG b) Z1-GG

Figure 14. SEM Images of sample a) STD-OG b) Z1-OG

Figure 15 – EDS spectra of Figure 13: (a) crystals (black circles of Figure 13) (b) glassy phase

Table 1 – Formulation of white standard frit (STD-F) (wt%)

Raw materials	STD – F (wt%)
Borax pentahydrate	16.8
Zircon	7.2
Dolomite	6.2
K-feldspar	32.5
Feldspatic flour	37.3

For Peer Review

Table 2 – Formulation of white standard glazes: STD-GG and STD-OG (wt%)

Raw materials	STD – GG (wt%)	STD – OG(wt%)
Frit	9	10
Frit 2	1	0
Zircon	17	17
White Clay	22	22
Alumina	4	4
Caolin	10	10
Calcium Carbonate	11	11
Nepheline	24.5	24.5
Zinc Oxide	1.5	1.5

For Peer Review

Table 3 – Properties of the as-received Zirconia powders Z1AR and Z2AR

Properties	Z1AR	Z2AR
<u>Grain size parameters (<math>\mu\text{m}</math>)</u>		
D10	20	3
D50	38	18
D90	67	54
<u>XRF (wt%)</u>		
ZrO <sub>2</sub>	85,0	79,7
Y <sub>2</sub> O <sub>3</sub>	9,3	8,6
HfO <sub>2</sub>	3,4	3,1
NiO	-	2,5
Cr <sub>2</sub> O <sub>3</sub>	-	2,1
Al <sub>2</sub> O <sub>3</sub>	0,7	1,3
Co <sub>3</sub> O <sub>4</sub>	-	0,8
SiO <sub>2</sub>	0,5	1,1
Na <sub>2</sub> O	0,3	0,4
Others	0,8	0,4
<u>Colorimetric Parameters</u>		
L*	91,85 $\pm$ 1,34	84,03 $\pm$ 0,98
a*	-0,94 $\pm$ 0,22	-1,09 $\pm$ 0,12
b*	18,46 $\pm$ 0,02	13,92 $\pm$ 0,42

Table 4 – Properties of the sieved fraction of Z1AR

Properties	<38 $\mu$ m	>38 $\mu$ m	>45 $\mu$ m	>75 $\mu$ m
Sieved fraction (% Z1AR)	59.16	10.00	28.96	11.64
Grain size parameters ( $\mu$ m)				
D10	10	27	36	12
D50	20	38	52	72
D90	36	54	76	132
XRF (wt%)				
ZrO <sub>2</sub>	85.6	84.8	84.3	82.6
Y <sub>2</sub> O <sub>3</sub>	9.3	9.4	9.2	9.1
HfO <sub>2</sub>	3.2	3.1	3.3	3.1
NiO	-	-	-	-
Cr <sub>2</sub> O <sub>3</sub>	-	-	-	-
Al <sub>2</sub> O <sub>3</sub>	0.4	1.2	1.8	3.7
Co <sub>3</sub> O <sub>4</sub>	-	-	-	-
SiO <sub>2</sub>	0.4	0.3	0.3	0.3
Na <sub>2</sub> O	0.3	0.3	0.3	0.3
Others	0.8	0.9	0.8	0.9
Colorimetric Parameters				
L*	89.4 $\pm$ 0.27	88.90 $\pm$ 0.42	86.40 $\pm$ 0.34	83.00 $\pm$ 0.24
a*	-0.5 $\pm$ 0.04	-1.0 $\pm$ 0.07	-0.2 $\pm$ 0.05	-0.2 $\pm$ 0.03
b*	12.5 $\pm$ 0.23	12.90 $\pm$ 0.43	12.60 $\pm$ 0.24	11.30 $\pm$ 0.29

Optical Microscope Images 35x



Table 5 – Properties of the sieved fraction of Z2AR

Properties	<38 $\mu$ m	>38 $\mu$ m	>45 $\mu$ m	>75 $\mu$ m
Sieved fraction (% Z2AR)	13.21	48.58	40.58	13.21
Grain size parameters ( $\mu$ m)				
D10	11	30	43	70
D50	22	43	60	95
D90	40	61	83	128
XRF (wt%)				
ZrO <sub>2</sub>	83.6	81.8	80.6	79.4
Y <sub>2</sub> O <sub>3</sub>	9.1	9.0	8.7	8.8
HfO <sub>2</sub>	3.6	3.1	3.1	3.3
NiO	0.5	0.5	0.5	0.4
Cr <sub>2</sub> O <sub>3</sub>	0.3	0.3	0.3	
Al <sub>2</sub> O <sub>3</sub>	0.3	/	/	/
Co <sub>3</sub> O <sub>4</sub>	1.0	2.8	2.8	3.2
SiO <sub>2</sub>	0.8	0.9	2.5	3.1
Na <sub>2</sub> O	0.3	0.9	0.9	1.2
Others	0.5	0.6	0.6	0.6
Colorimetric Parameters				
L*	66.6 $\pm$ 0.07	68.80 $\pm$ 0.43	68.7 $\pm$ 0.24	68.5 $\pm$ 0.34
a*	-1.8 $\pm$ 0.10	-1.8 $\pm$ 0.05	-1.5 $\pm$ 0.08	-1.7 $\pm$ 0.02
b*	11.8 $\pm$ 0.25	12.50 $\pm$ 0.27	11.2 $\pm$ 0.45	13.60 $\pm$ 0.56
Optical Microscope Images 35x				



Table 6 – Hot stage microscope characterization of the frits

	Sintering (°C)	Softening (°C)	Sphere (°C)	Half sphere (°C)	Melting (°C)
STD-F	894	935	1109	1307	1338
Z1-F	803	1001	1151	1344	1377
Z2-F	794	877	1115	1306	1349

For Peer Review

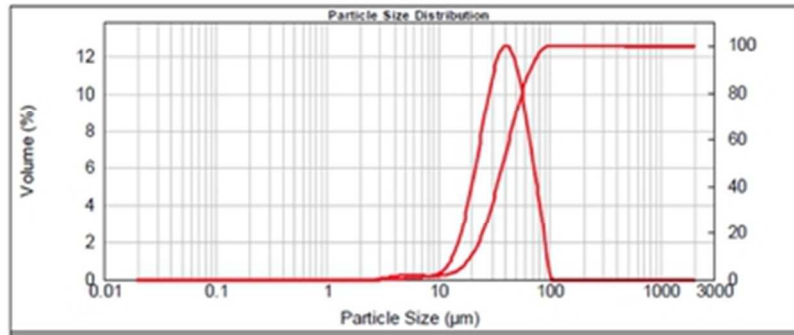
Table 7 – Hunter parameters of the frits investigated

FRITS	L*	a*	b*	$\Delta E$
STD -F	$88.73 \pm 0.14$	$-0.62 \pm 0.02$	$1.55 \pm 0.05$	/
Z1-F	$87.32 \pm 0.09$	$-0.64 \pm 0.12$	$1.11 \pm 0.13$	1.13
Z2-F	$70.45 \pm 0.11$	$-6.54 \pm 0.09$	$7.23 \pm 0.05$	20.04

For Peer Review

Table 8 – Hunter parameters of the glazes investigated

GLAZES	L*	a*	b*	$\Delta E$
<b>GLOSSY</b>				
STD - GG	$90.19 \pm 0.53$	$-0.66 \pm 0.03$	$-0.28 \pm 0.06$	/
Z1 - GG	$90.33 \pm 0.44$	$-0.70 \pm 0.07$	$0.43 \pm 0.12$	1.54
Z2 - GG	$73.18 \pm 0.09$	$-3.19 \pm 0.06$	$5.42 \pm 0.09$	18.12
<b>OPAQUE</b>				
STD - OG	$86.32 \pm 0.12$	$-0.65 \pm 0.03$	$0.83 \pm 0.04$	/
Z1 - OG	$86.41 \pm 0,16$	$0.66 \pm 0.02$	$0.92 \pm 0.04$	1.32
Z2 - OG	$70.18 \pm 0.23$	$-2.59 \pm 0.12$	$6.38 \pm 0.06$	17.37



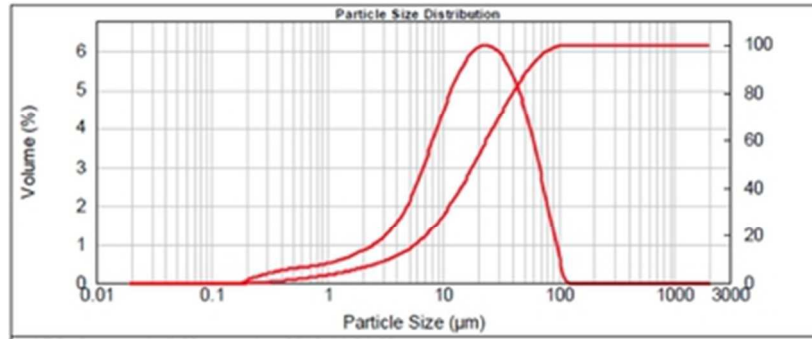
Grain size distribution of sample Z1AR

Figure 1

34x14mm (300 x 300 DPI)

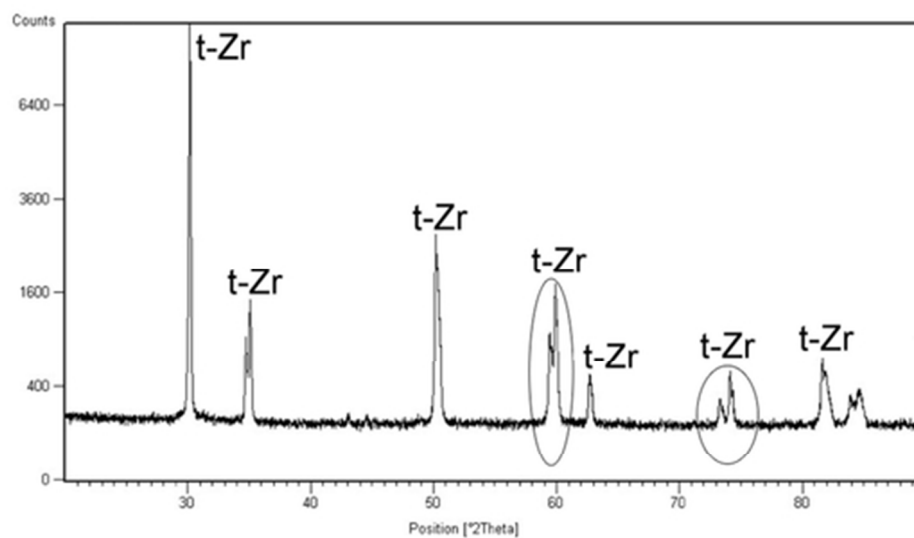
Peer Review

1  
2  
3  
4  
5  
6  
7  
8  
9  
10  
11  
12  
13  
14  
15  
16  
17  
18  
19  
20  
21  
22  
23  
24  
25  
26  
27  
28  
29  
30  
31  
32  
33  
34  
35  
36  
37  
38  
39  
40  
41  
42  
43  
44  
45  
46  
47  
48  
49  
50  
51  
52  
53  
54  
55  
56  
57  
58  
59  
60

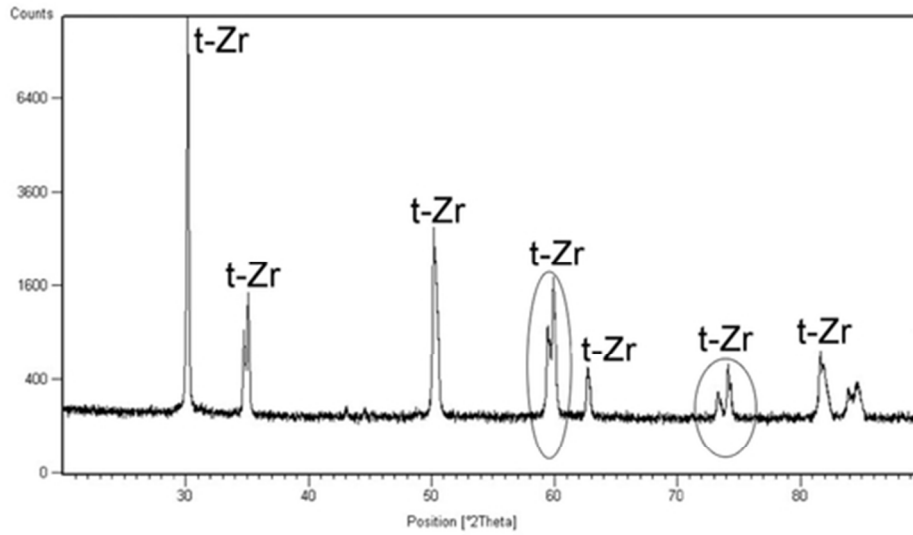


Grain size distribution of sample Z2AR  
Figure 2  
34x14mm (300 x 300 DPI)

Peer Review



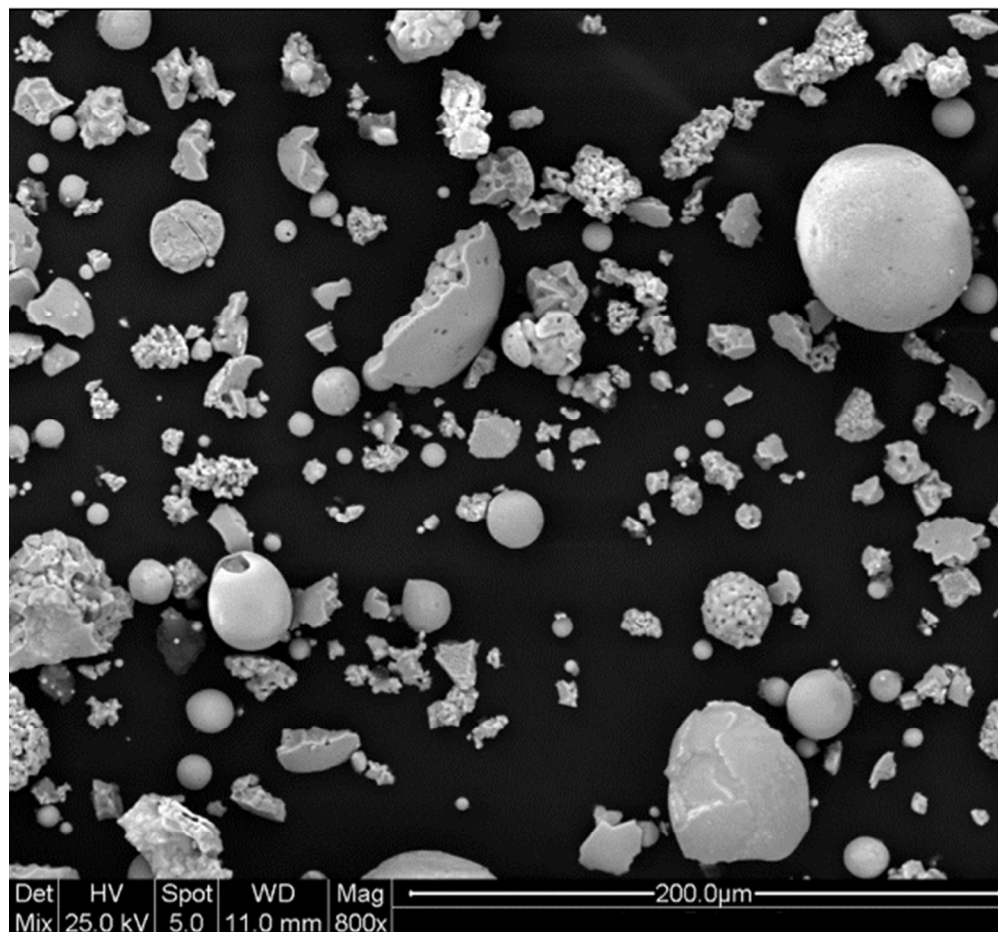
XRD Pattern of sample Z1AR: t-Zr, tetragonal zirconia  
Figure 3  
47x26mm (300 x 300 DPI)



XRD Pattern of sample Z2AR: t-Zr, tetragonal zirconia  
Figure 4  
47x26mm (300 x 300 DPI)

er Review

1  
2  
3  
4  
5  
6  
7  
8  
9  
10  
11  
12  
13  
14  
15  
16  
17  
18  
19  
20  
21  
22  
23  
24  
25  
26  
27  
28  
29  
30  
31  
32  
33  
34  
35  
36  
37  
38  
39  
40  
41  
42  
43  
44  
45  
46  
47  
48  
49  
50  
51  
52  
53  
54  
55  
56  
57  
58  
59  
60



1  
2  
3  
4  
5  
6  
7  
8  
9  
10  
11  
12  
13  
14  
15  
16  
17  
18  
19  
20  
21  
22  
23  
24  
25  
26  
27  
28  
29  
30  
31  
32  
33  
34  
35  
36  
37  
38  
39  
40  
41  
42  
43  
44  
45  
46  
47  
48  
49  
50  
51  
52  
53  
54  
55  
56  
57  
58  
59  
60

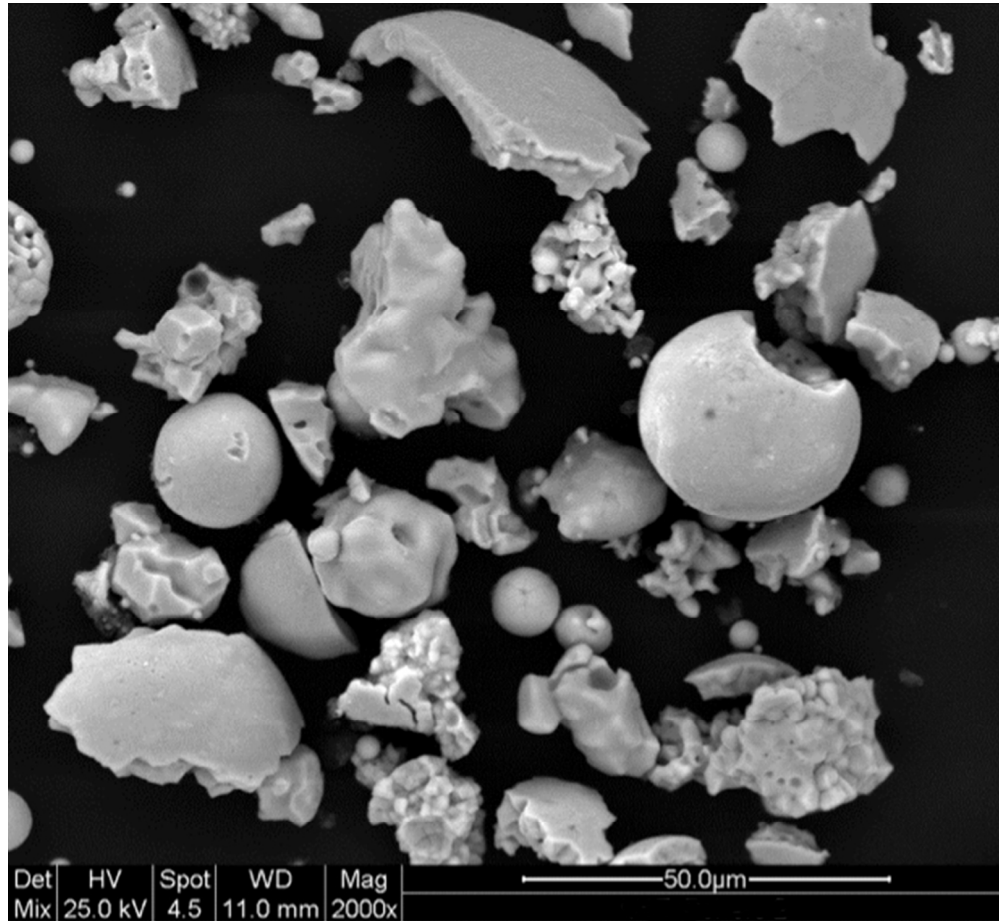


Figure 5. SEM Images at different magnitude of sample Z1AR  
Figure 5  
85x78mm (300 x 300 DPI)



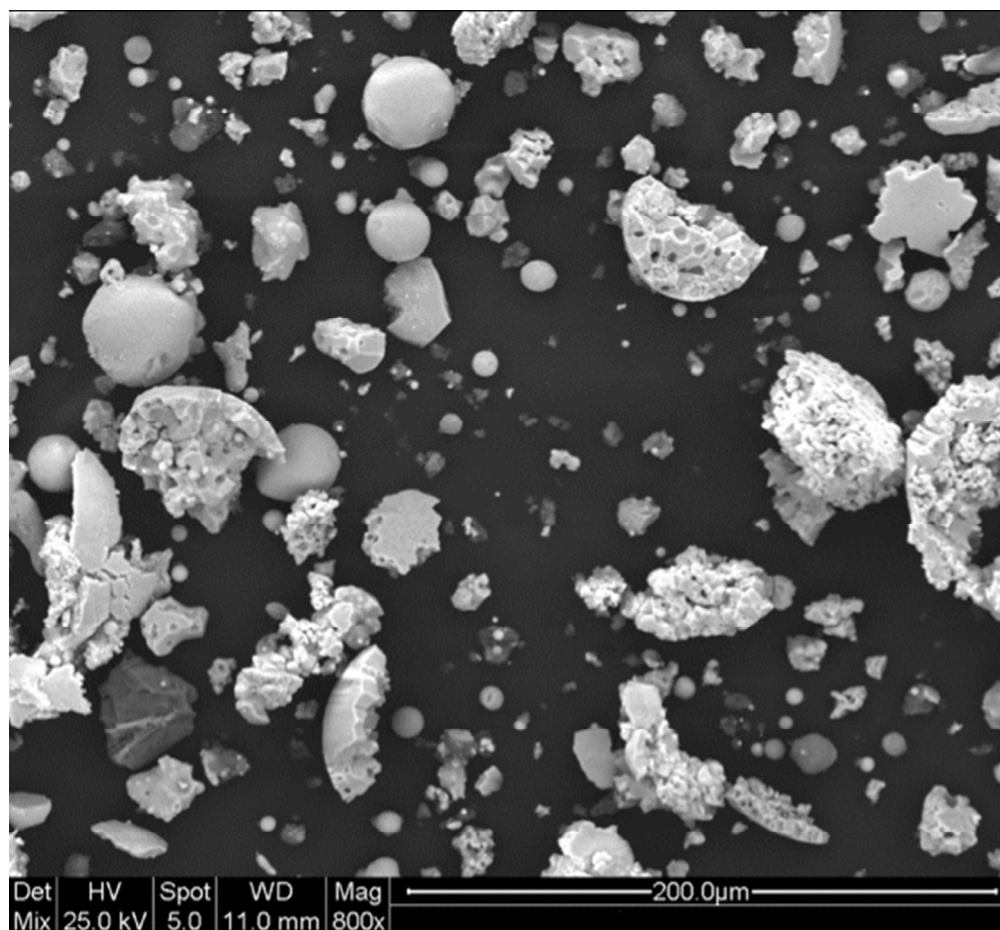


Figure 6. SEM Images at different magnitude of sample Z2AR

Figure 6

85x78mm (300 x 300 DPI)



1  
2  
3  
4  
5  
6  
7  
8  
9  
10  
11  
12  
13  
14  
15  
16  
17  
18  
19  
20  
21  
22  
23  
24  
25  
26  
27  
28  
29  
30  
31  
32  
33  
34  
35  
36  
37  
38  
39  
40  
41  
42  
43  
44  
45  
46  
47  
48  
49  
50  
51  
52  
53  
54  
55  
56  
57  
58  
59  
60

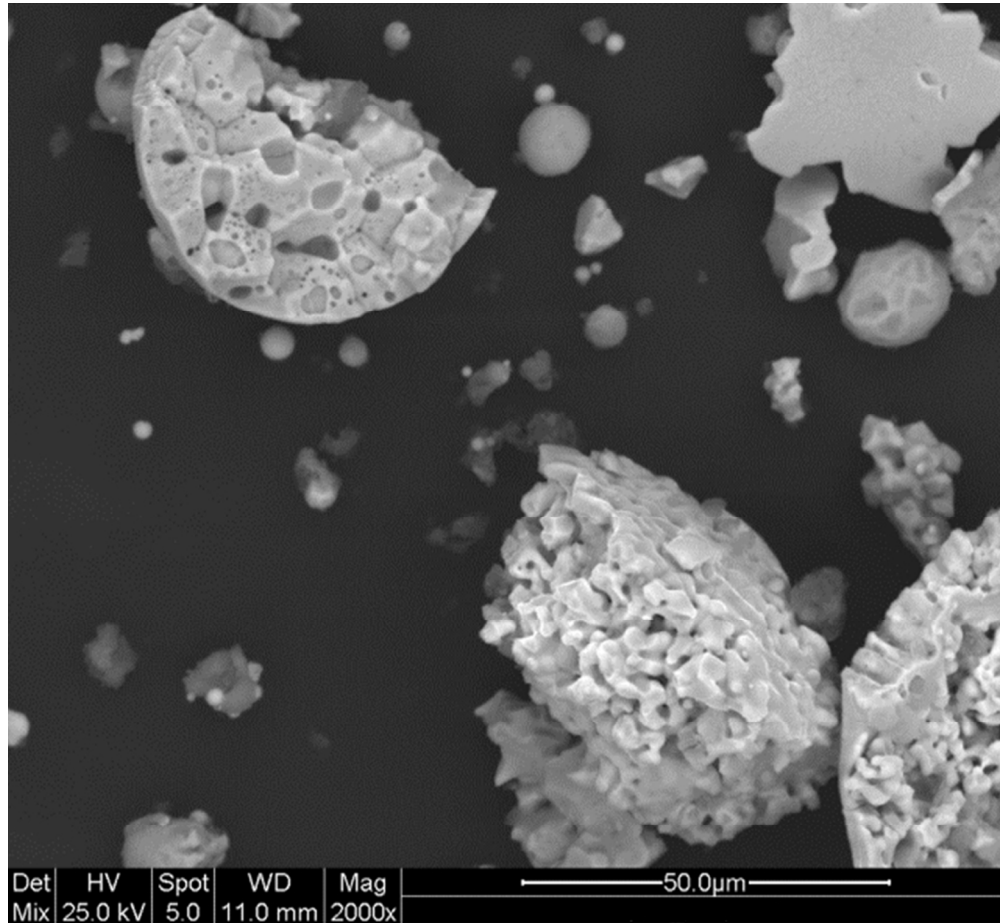


Figure 6. SEM Images at different magnitude of sample Z2AR  
Figure 6  
85x78mm (300 x 300 DPI)



1  
2  
3  
4  
5  
6  
7  
8  
9  
10  
11  
12  
13  
14  
15  
16  
17  
18  
19  
20  
21  
22  
23  
24  
25  
26  
27  
28  
29  
30  
31  
32  
33  
34  
35  
36  
37  
38  
39  
40  
41  
42  
43  
44  
45  
46  
47  
48  
49  
50  
51  
52  
53  
54  
55  
56  
57  
58  
59  
60

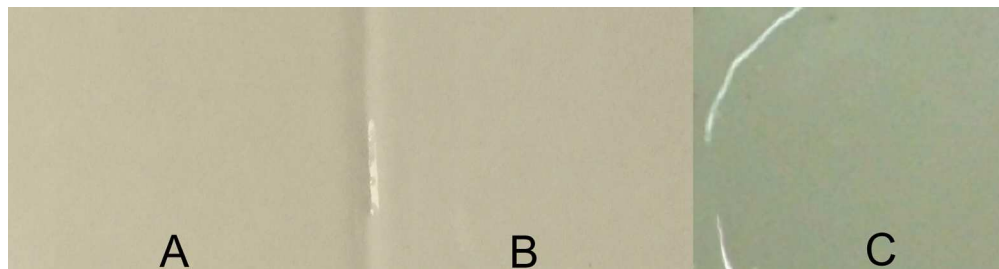


Figure 7. Comparison of the glossy glazes obtained a) STD-GG b) Z1-GG c) Z2-GG

Figure 7  
177x46mm (300 x 300 DPI)

For Peer Review

1  
2  
3  
4  
5  
6  
7  
8  
9  
10  
11  
12  
13  
14  
15  
16  
17  
18  
19  
20  
21  
22  
23  
24  
25  
26  
27  
28  
29  
30  
31  
32  
33  
34  
35  
36  
37  
38  
39  
40  
41  
42  
43  
44  
45  
46  
47  
48  
49  
50  
51  
52  
53  
54  
55  
56  
57  
58  
59  
60

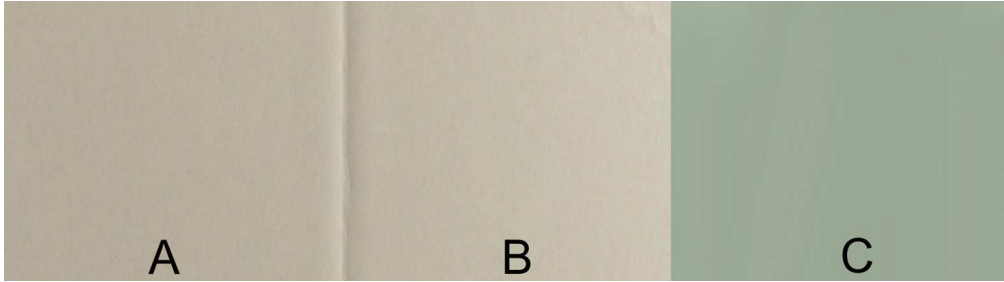


Figure 8. Comparison of the opaque glazes obtained a) STD-OG b) Z1-OG c) Z2-OG  
Figure 8  
177x49mm (300 x 300 DPI)

Or Peer Review

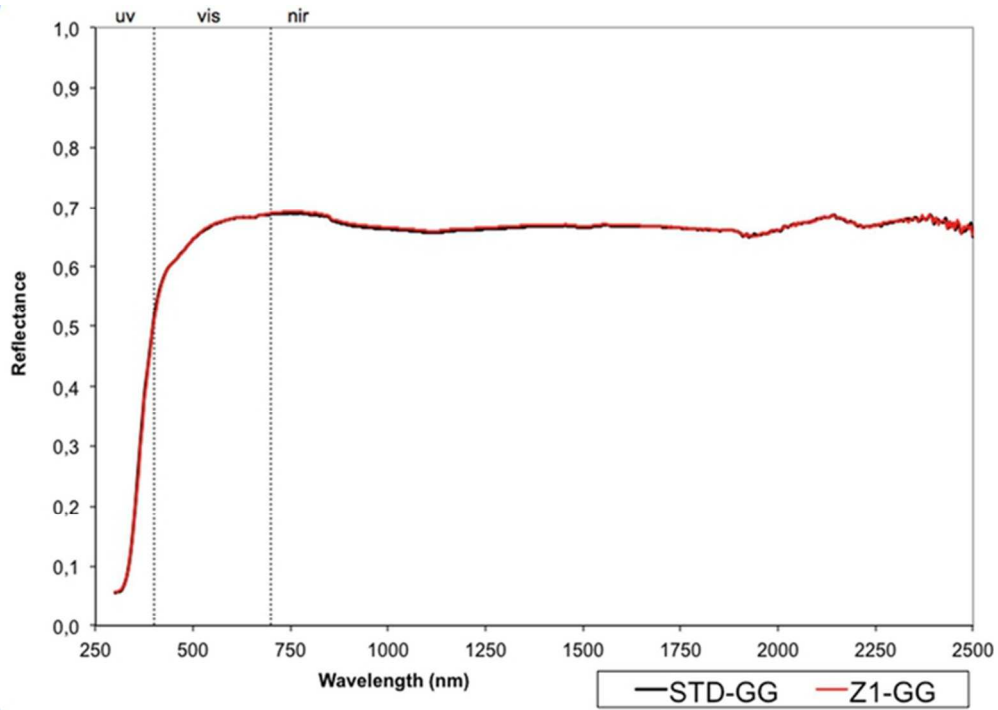


Figure 9. Reflectance spectra of the white glossy glazes

Figure 9

60x43mm (300 x 300 DPI)

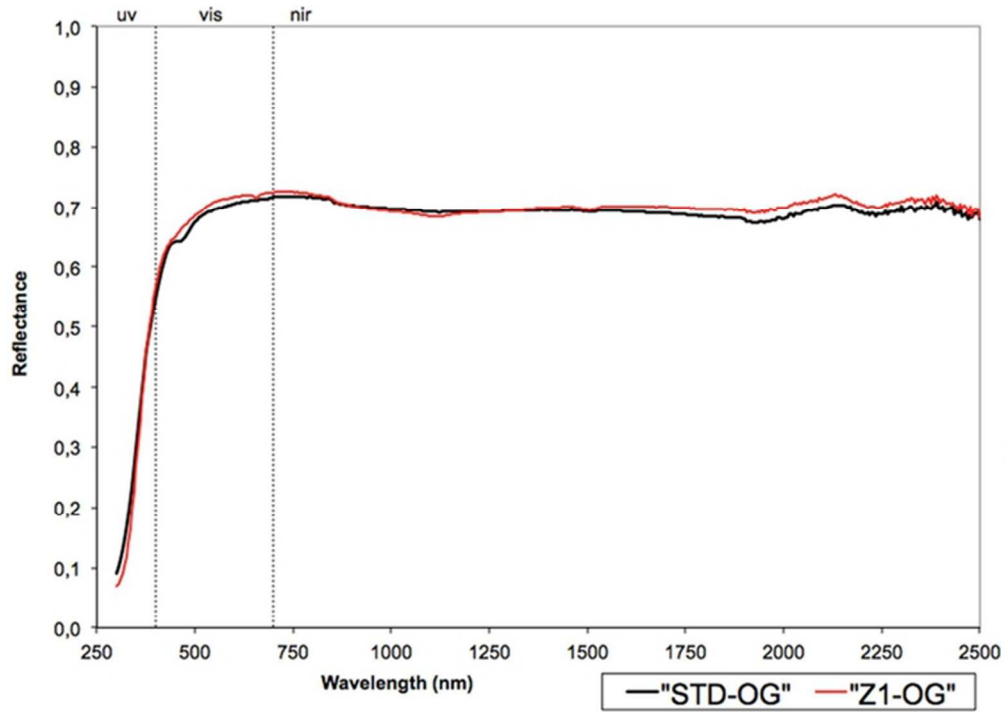


Figure 10. Reflectance spectra of the white opaque glazes  
Figure 10  
60x43mm (300 x 300 DPI)

Review

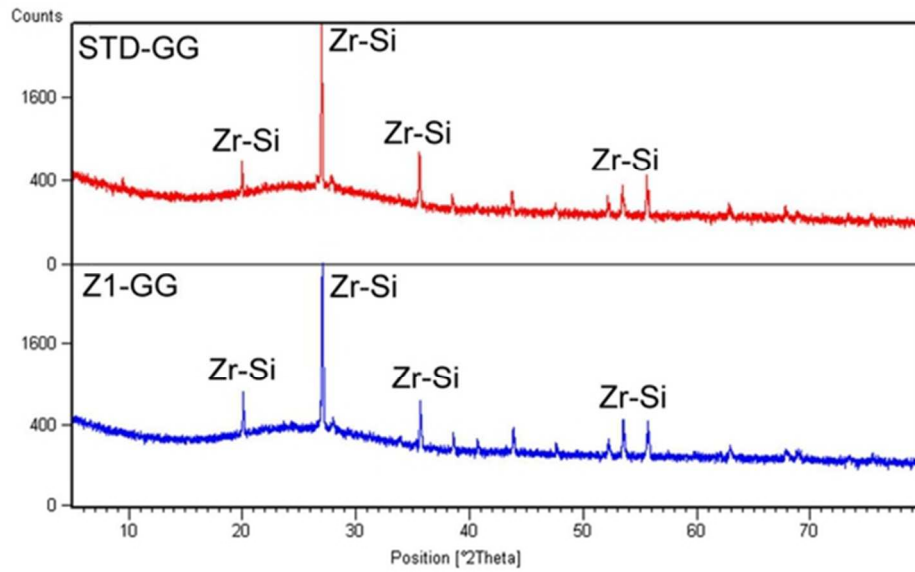


Figure 11. XRD Pattern of the white glossy glazes: Zr-Si, Zirconium Silicate

Figure 11

53x33mm (300 x 300 DPI)

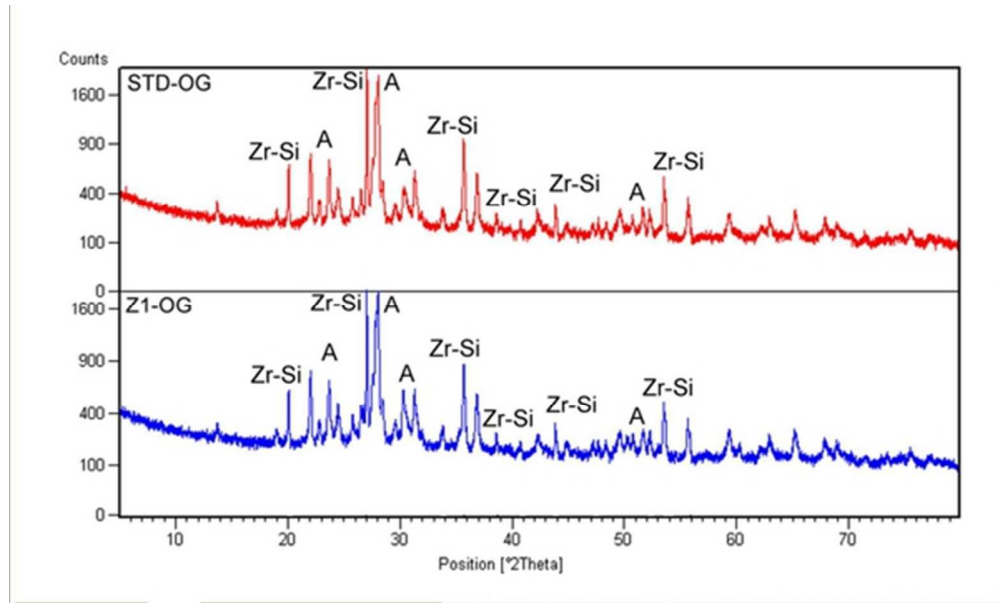


Figure 12. XRD Pattern of the white opaque glazes: Zr-Si, Zirconium Silicate; A, Anorthite  
Figure 12  
50x30mm (300 x 300 DPI)

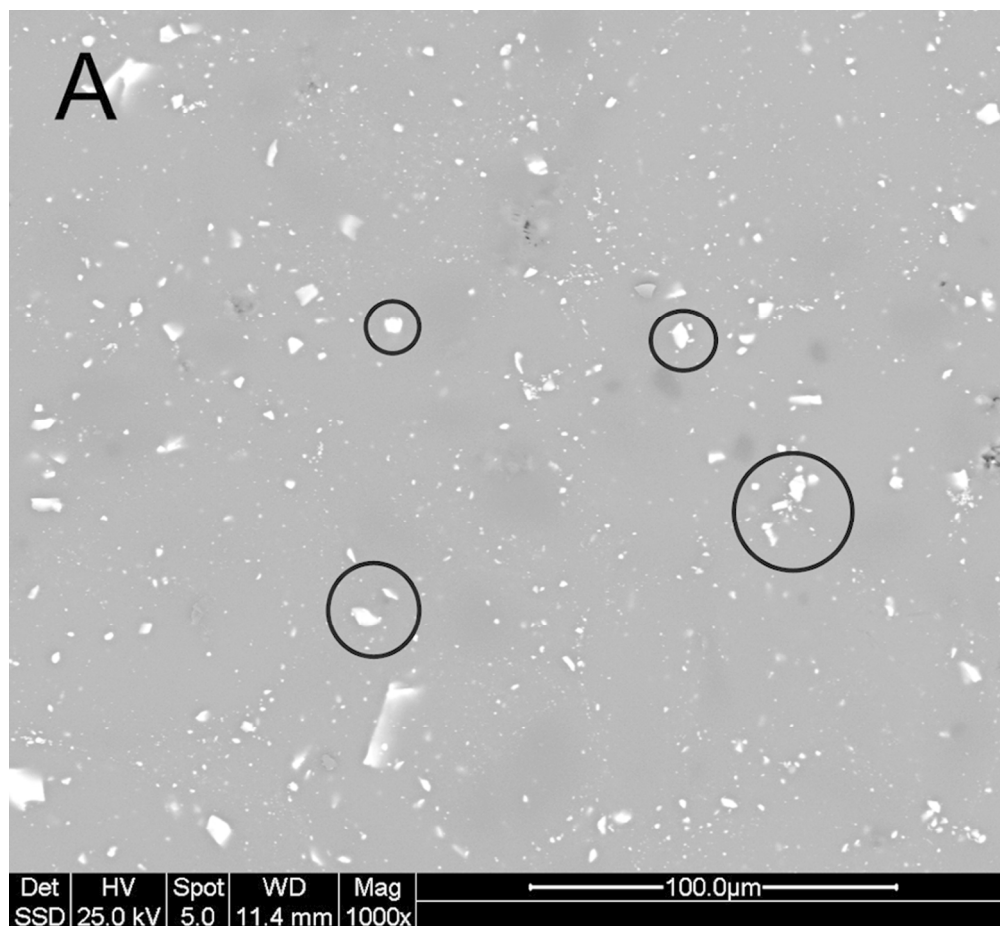


Figure 13. SEM Images of sample a) STD-GG b)Z1-GG

Figure 13

85x78mm (300 x 300 DPI)



1  
2  
3  
4  
5  
6  
7  
8  
9  
10  
11  
12  
13  
14  
15  
16  
17  
18  
19  
20  
21  
22  
23  
24  
25  
26  
27  
28  
29  
30  
31  
32  
33  
34  
35  
36  
37  
38  
39  
40  
41  
42  
43  
44  
45  
46  
47  
48  
49  
50  
51  
52  
53  
54  
55  
56  
57  
58  
59  
60

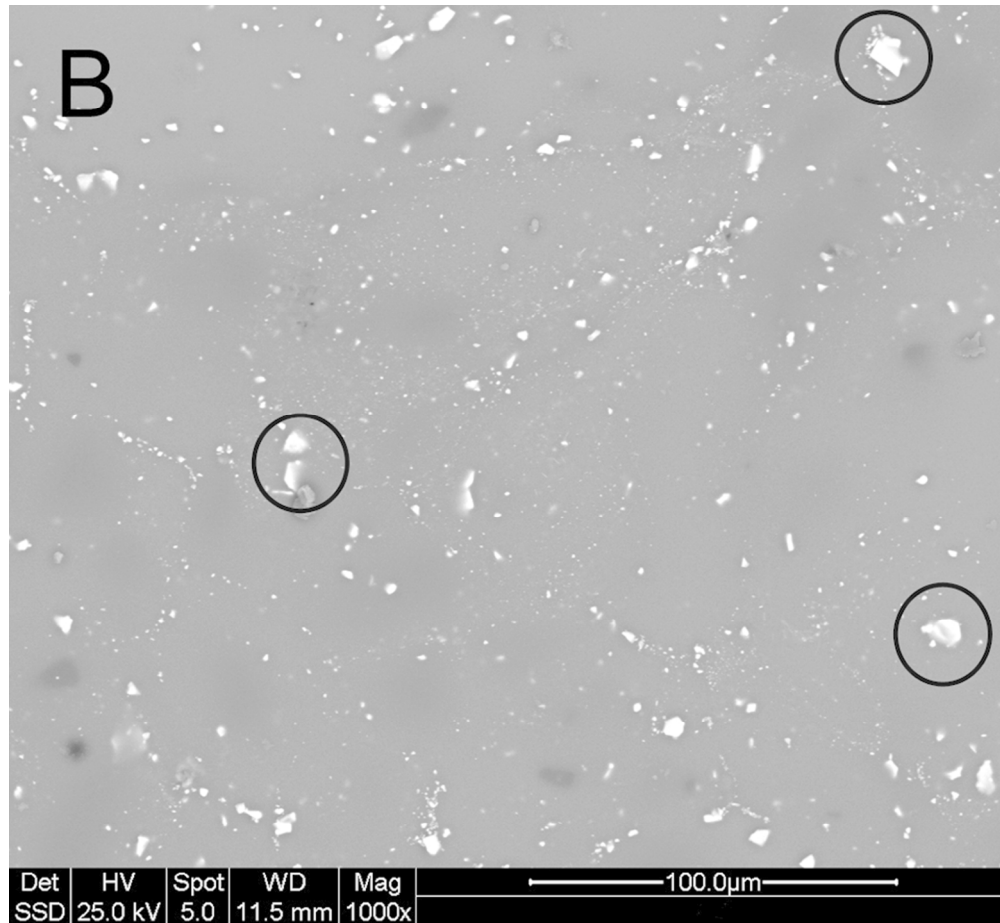


Figure 13. SEM Images of sample a) STD-GG b)Z1-GG

Figure 13

85x78mm (300 x 300 DPI)



1  
2  
3  
4  
5  
6  
7  
8  
9  
10  
11  
12  
13  
14  
15  
16  
17  
18  
19  
20  
21  
22  
23  
24  
25  
26  
27  
28  
29  
30  
31  
32  
33  
34  
35  
36  
37  
38  
39  
40  
41  
42  
43  
44  
45  
46  
47  
48  
49  
50  
51  
52  
53  
54  
55  
56  
57  
58  
59  
60

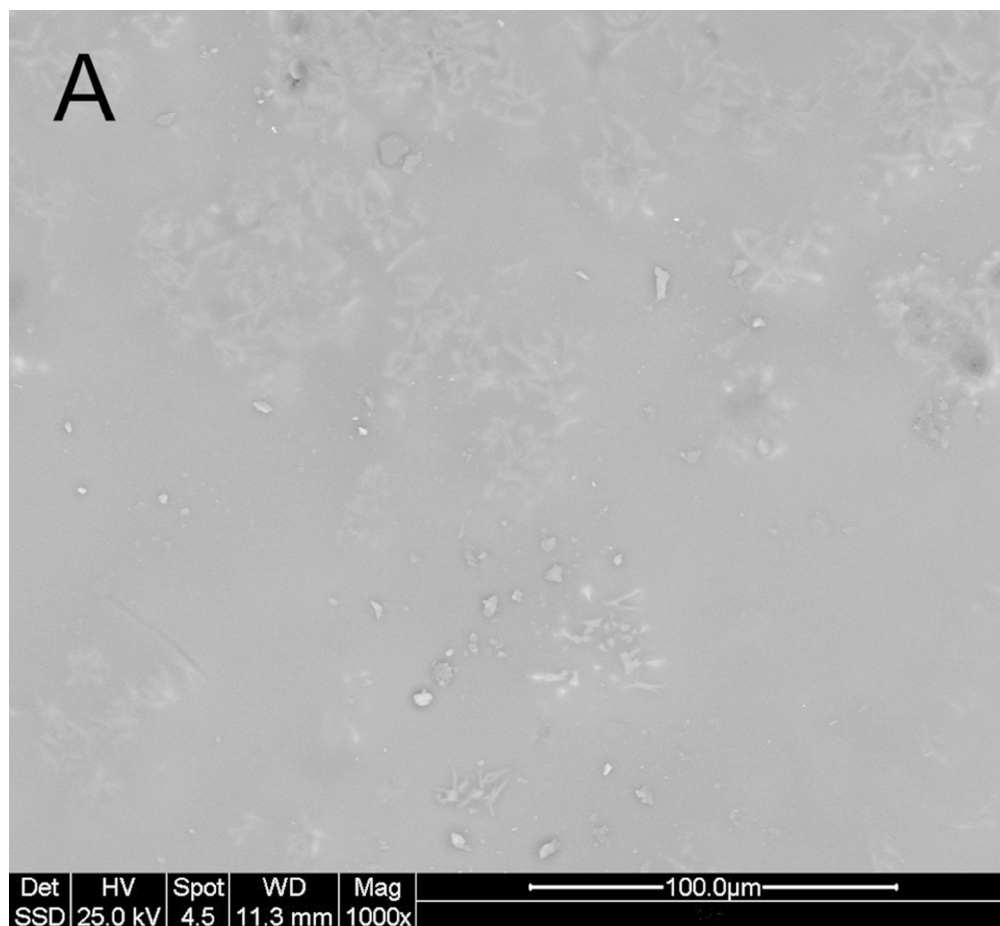


Figure 14. SEM Images of sample a) STD-OG b)Z1-OG  
Figure 14  
85x78mm (300 x 300 DPI)



1  
2  
3  
4  
5  
6  
7  
8  
9  
10  
11  
12  
13  
14  
15  
16  
17  
18  
19  
20  
21  
22  
23  
24  
25  
26  
27  
28  
29  
30  
31  
32  
33  
34  
35  
36  
37  
38  
39  
40  
41  
42  
43  
44  
45  
46  
47  
48  
49  
50  
51  
52  
53  
54  
55  
56  
57  
58  
59  
60

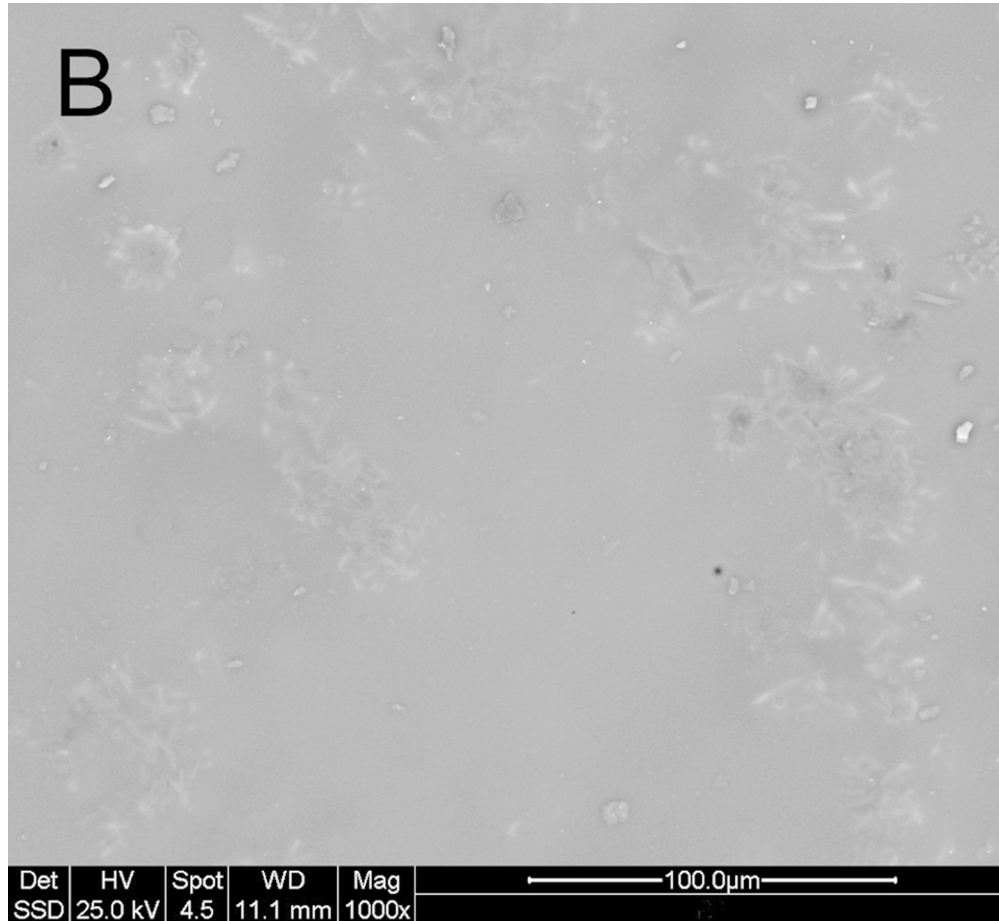


Figure 14. SEM Images of sample a) STD-OG b)Z1-OG  
Figure 14  
85x78mm (300 x 300 DPI)



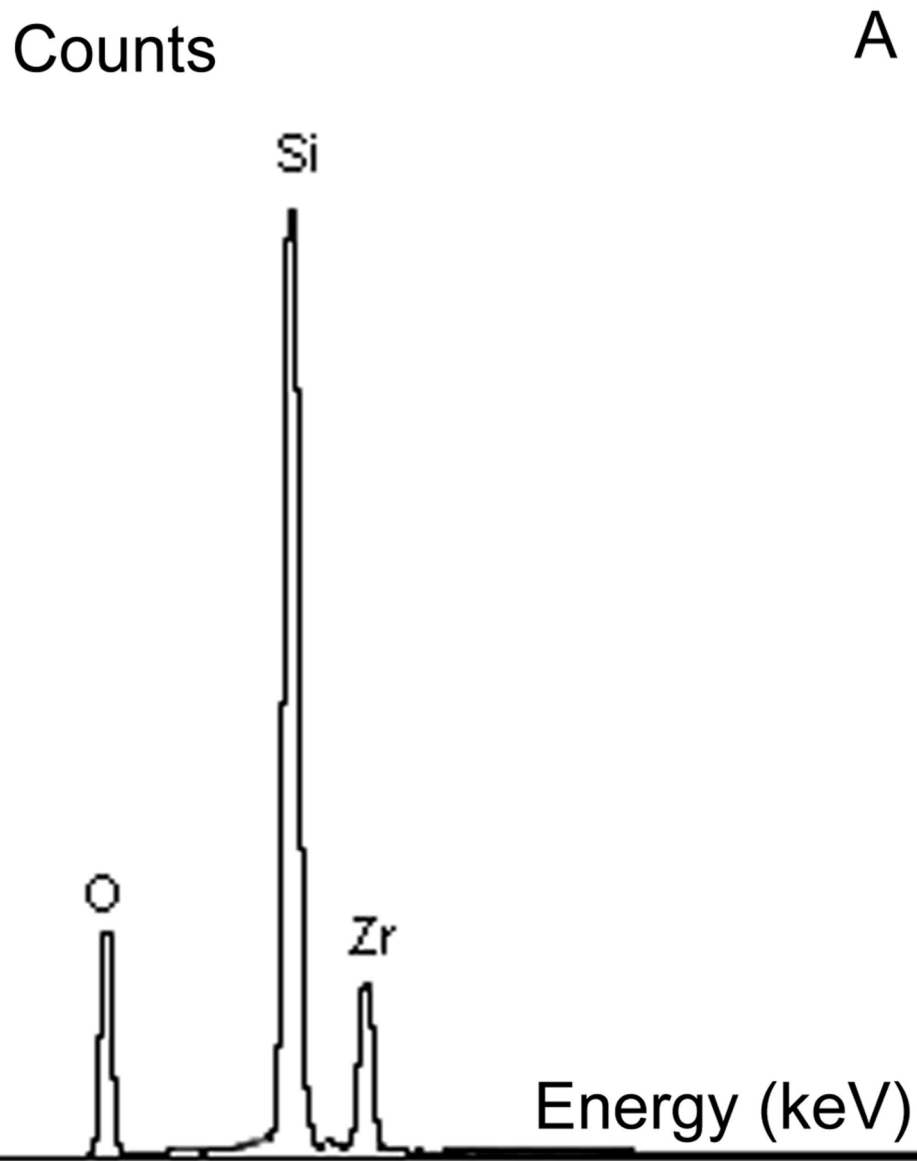


Figure 15 – EDS spectra of Figure 13: (a) crystals (black circles of Figure 13) (b) glassy phase  
Figure 15

110x144mm (300 x 300 DPI)

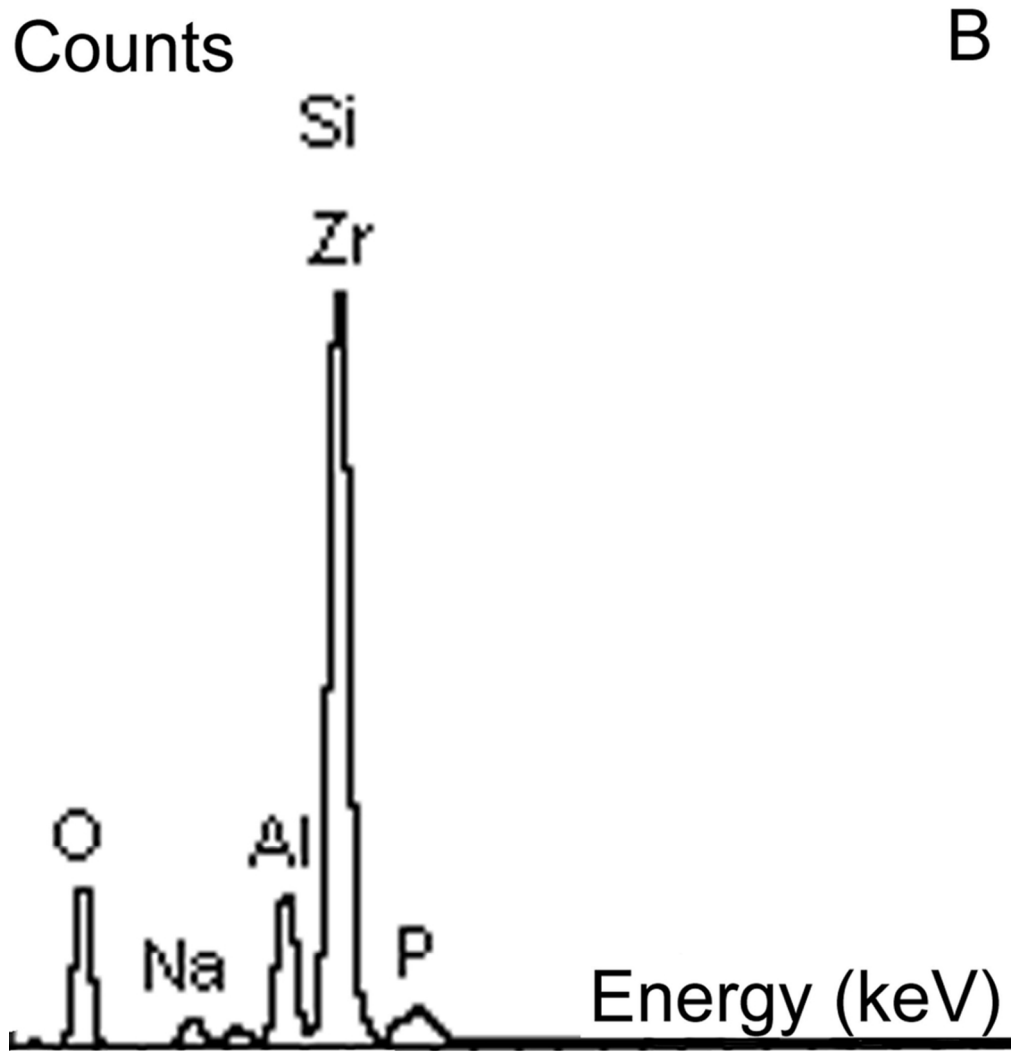


Figure 15 - EDS spectra of Figure 13: (a) crystals (black circles of Figure 13) (b) glassy phase  
Figure 15  
90x97mm (300 x 300 DPI)